ARTICLE   OPEN

A soft and stretchable electronics using laser-induced graphene on polyimide/PDMS composite substrate

Hao Wang[1], Zifen Zhao[1], Panpan Liu[1] and Xiaogang Guo [ID][1 ✉]

The one-step fabricated laser-induced graphene (LIG) has the advantages of low cost, patterning of various desired geometries, and high sensitivity. However, the robustness of substrates imposes certain constraints on their applications in stretchable devices. In this paper, the substrate composed of polydimethylsiloxane (PDMS) and polyimide (PI) particles is proposed to serve as the platform to manufacture LIG. Ascribing to the inherent soft and stretchable attributes of the PI/PDMS composite substrate, the LIG-based sensors can fit complex 3D configurations or bear a mechanical tension over 15%. Notably, the fluence of the laser is experimentally and theoretically determined as the only principle to characterize the formation of conductive LIG on PI/PDMS composite greatly facilitating the selection of the allowable laser scanning parameters to form the desired LIG-based devices. Three demonstrations are conducted to highlight the superiority and the potential of this soft and stretchable LIG-based system in wearable electronics and soft robots.

INTRODUCTION

The organic films can be photothermally converted to continuous 3D porous graphene structures by pulsed laser irradiation under air, known as the formation procedure of laser-induced graphene (LIG). Recent researches have reported that laser-induced graphene (LIG) can be successfully prepared on many kinds of natural and synthetic materials that with sufficient carbon sources, such as woods[1,2], clothes[3–5], coconut shell[5], commercial polyimide (PI)[6–31], and even official paper[32–34]. Here, the commercial laser cutting machine equipped with a CO_2 laser beam often serves as the primary manufacturing platform of LIG on some specific substrates. The underlying mechanisms mainly involve the carbonization and graphitization occurring on the surface of these substrates. The sharp rise in the localized temperature due to lattice vibrations by the laser irradiation easily breaks the C-O, C=O, and N-C bond, and the material goes through a transition from an sp3- to sp2-hybridized state. CO gas is evolved during the polymer to amorphous structure conversion, and H_2 gas is evolved throughout the photo-thermal conversion process. The aromatic compounds are then rearranged to form graphitic structures due to the recombination of the C-C bond[6,35]. According to this strategy, any desired complex graphene pattern can be directly formed on the carbon sources films, facilitating the fabrication procedures for the individually customized electrical devices. The ambient manufacturing condition, well-designed digital models by computer-aided design (CAD), various allowable materials with sufficient carbon source as substrates promise the LIG-based system as a one-step, straightforward and facile way for the controllable formation of flexible electronics and piezoresistive sensors for wearable electronics[7,10,22,23,27,29,36–39], and other applications, such as nanogenerators[40,41], capacitors[11,13,20,42], heaters[8], catalyst[43], actuators[25,26], battery electrodes[14,44,45], and antiviral materials[46]. Now, the commercial PI film is the most common substrate to form the high-quality LIG, ascribing to its thermal-mechanical stability and rich carbon content. However, the limitation from its in-plane robustness imposes certain constraints on their applications for the devices that require a

high stretchability. Stretchable substrates and devices obtained through material and structural design are essential for wearable electronics[47–52]. The maximum strain for the LIG-based sensor fabricated on the PI film is less than 3% before broken, far below the allowable strain of human skin (i.e., >13%). From this perspective, it is still challenging to manufacture LIG-based electronics with wide available stretchability (i.e., >15%). To address this increasing demand, a stretchable and sticky polydimethylsiloxane (PDMS) that can be achieved by a simple process is an ideal elastic substrate for improving the stretchability of LIG-based devices. Benefiting from its characteristics, transferring the LIG from the PI substrate onto the stretchable PDMS substrate can significantly enlarge the accessible strain range of the flexible strain sensor, and PI/PDMS composite can be used as substrates for flexible sensors and flexible supercapacitors[53,54]. Inspired by relevant research, the substrates composed of PDMS and PI particles are prepared, serving as the soft and stretchable platform to form the laser-induced graphene. Here, a specific concentration of PI particle poured into the PDMS solution offers the required carbon source for forming porous graphene under the irradiation of an infrared laser beam. At the same time, PDMS promises the soft and stretchable performances of this LIG-based system. In general, various manufacturing parameters can be divided into two categories, the material composition (i.e., the weight ratio of PI particle to PDMS) and the conditions of the laser scanning procedure (i.e., the laser power, the frequency, the scanning speed and the dots per inch (DPI)). All of them offer great influences on the electrical and mechanical performances of the LIG-based system, which have been measured and analyzed by mechanical tension experiments and SEM images. Thus, the influences of those parameters mentioned above on the conductivity of LIG are experimentally measured and analyzed through their corresponding SEM images. Notably, the fluence of the laser is finally experimentally and theoretically determined as the only principle to characterize the formation of conductive LIG on PI/PDMS composite substrate, and greatly facilitates the selection of the laser scanning parameters (i.e., laser power,

[1]Institute of Advanced Structure Technology, Beijing Institute of Technology, Beijing 100081, China. ✉email: guoxg@bit.edu.cn
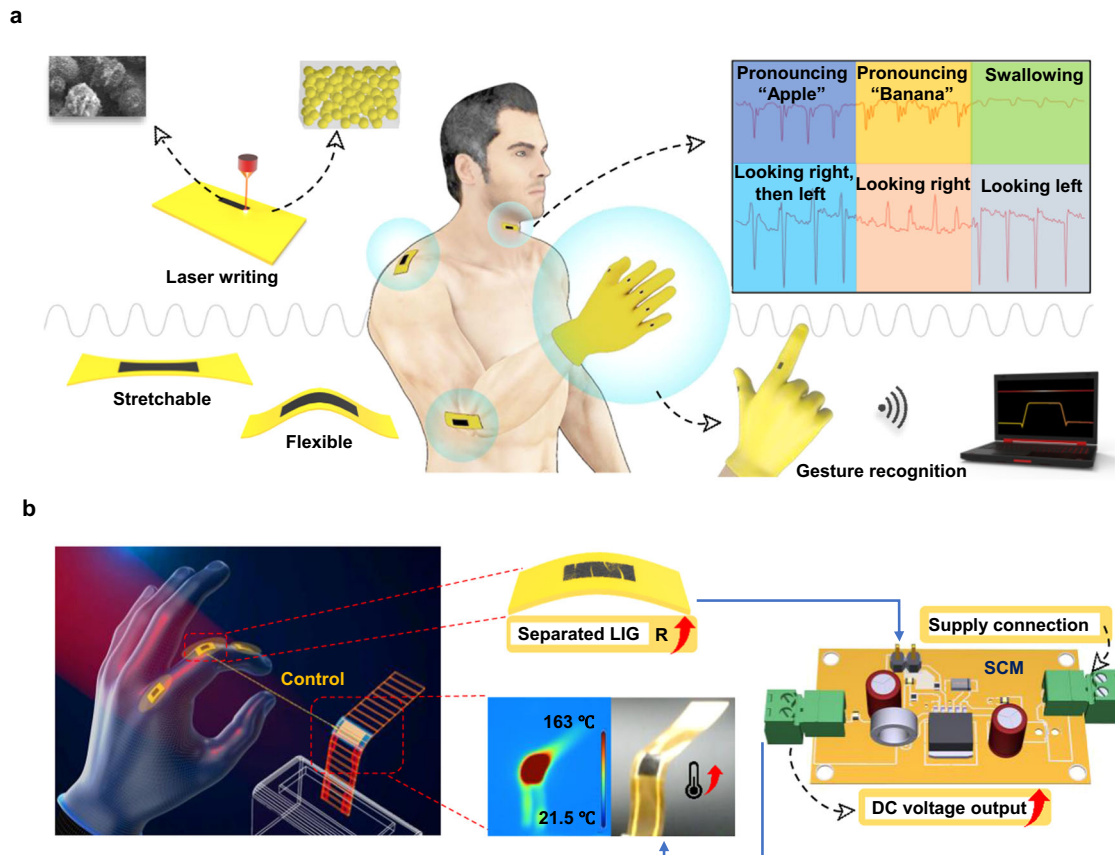
a

b

Fig. 1 Schematic illustration of the soft and stretchable LIG-based sensor as the wearable electronic. a The application of the LIG-based sensors as the wearable electronics to monitor the human electrophysiological activities. **b** Working mechanism of LIG-based sensor as a tool to remotely control an actuator.

frequency, scanning speed and DPI). For the demonstrations of the LIG-based system as the wearable sensor and the remote controller, three examples (i.e., the sensor of electrophysiological activities, the monitor of finger motion and the tool of the real-time actuators control) are conducted, respectively. Here, the soft and wearable LIG-based sensors are adhered onto the wrist to monitor the pulse rate wave, and the throat to record the pronunciation and head motion, respectively. Furthermore, the LIG-based soft glove is fabricated to monitor the gestures of one hand, and to serve as a wearable tool for the remote control of actuators.

RESULTS

Property characterization of the LIG-based sensor

Figure 1a depicts the potential of the soft and stretchable LIG-based electrical system in the fields of wearable electronics ascribing to its high sensitivity in monitoring a slight deformation. The LIG-based sensors fabricated on the PI/PDMS composite thin films or gloves under the irradiation of laser beam can be mounted to the shoulder, elbow and fingers to recognize the real-time bending deformations of these joints, and record the pulse rate wave after tightly adhered onto the wrists. As shown in the upper right corner of Fig. 1a and Supplementary Fig. 1, the soft and stretchable LIG-based sensor is mounted onto the volunteer's throat for recognizing pronunciation and recording the head motion. The porous structures and the high sensitivity of LIG enable its capability in sound detection according to the variation of the resistance caused by the vibration of the throat cords. The words Apple and Banana can be detected clearly. The sensor can also recognize the swallowing activity of the tester. Since the LIG

sensor is attached to the center-left of the neck, rotating the neck to different sides leads to the compression or stretch of the LIG devices, resulting in the decrease or increase of the resistance. Furthermore, a variety of soft and stretchable LIG-based sensors fabricated on PI/PDMS composites substrate can also be designed as the remote controller of soft robots. Figure 1b depicts the working mechanism of LIG-based sensor on soft and stretchable PI/PDMS composite substrate as the remote real-time wearable controller of an actuator. Here, the actuator is composed of a PI thin film (thickness: 75 μm) with fabricated LIG and PDMS layer (thickness: 300 μm), as shown in Supplementary Fig. 2a. The LIG herein serves as an electrical heater and the mismatch in the thermal strain between PI film and PDMS substrate yields the bending deformation of the actuator. And a higher input voltage of the actuator results in a larger bending angle. Through the single-chip microcomputer (SCM) (as shown in Supplementary Fig. 2b), the variation of the LIG-based sensor's resistance, highly related to the bending angle of the joint of the finger, are recognized and automatically converted into the input voltage of the actuator to control its bending motion. As illustrated in Supplementary Fig. 3a, the preparation of soft and stretchable LIG-based sensor fabricated on the PI/PDMS composite substrate begins with mixing and stirring the PI particle and PDMS solution under air. The PDMS solution used in this paper is Sylgard 184 from Dow Corning, a well-proportioned mixture of silicone elastomer base and curing agent in a weight ratio of 10:1. To determine the increase in carbon content in the composite, a tube furnace was used to carbonize the PDMS and PI/PDMS composite at 800 °C in N_2, and the weights of these materials before and after carbonization were illustrated in Supplementary Table 1, According to the experimental results, it showed that adding PI can
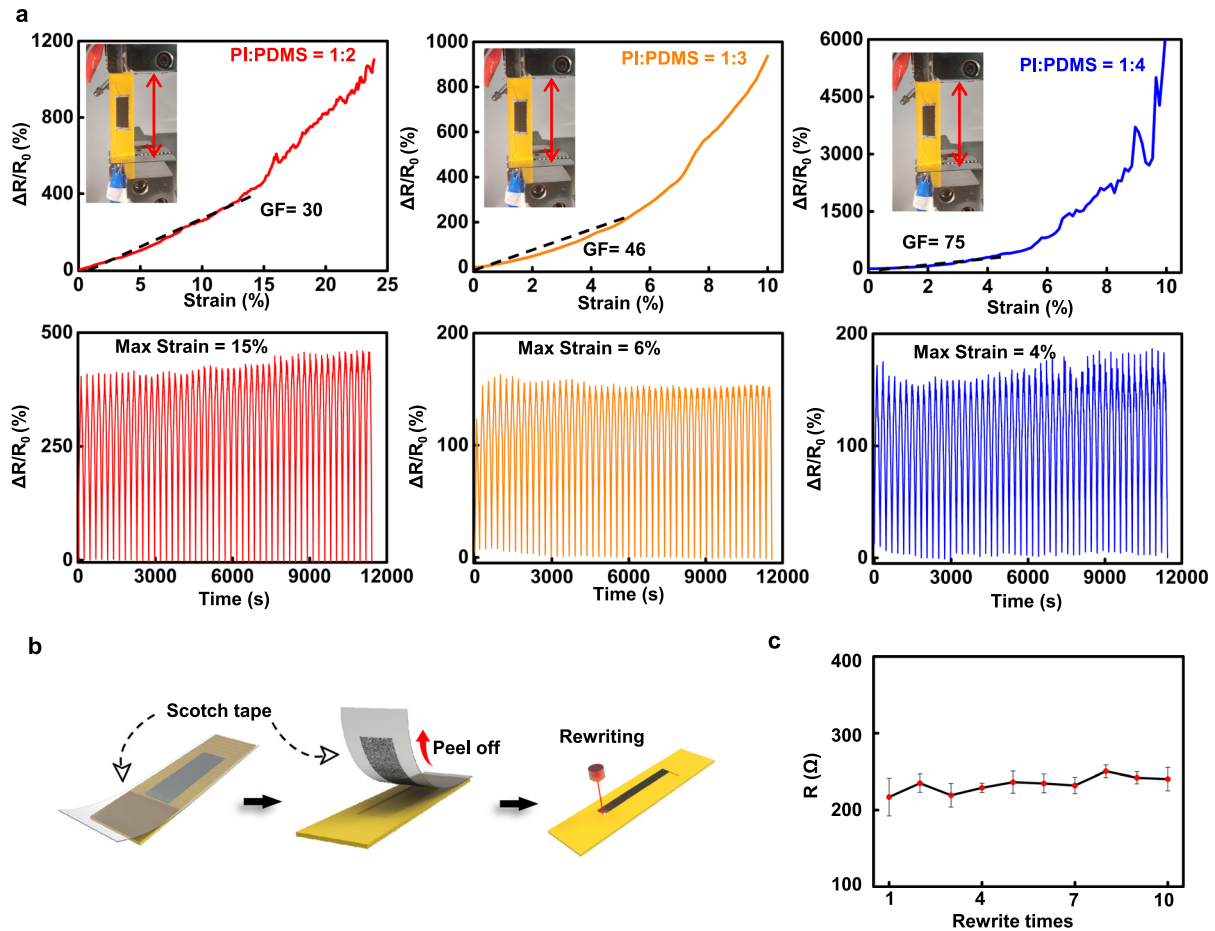
Fig. 2 The stretchability and recyclability of the soft and stretchable LIG-based sensor. a The normalized resistance versus the tensile strain for the LIG-based sensors fabricated on three PI/PDMS composite substrates with different PI to PDMS weight ratios (i.e., 1:2, 1:3 and 1:4 from left to right). The LIG-based sensors are fabricated onto PI/PDMS composite substrates under the irradiation condition of (specific power, frequency, scanning speed, DPI) = (12%, 16 kHz, 200 mm s^{-1}, 500). **b** Schematic illustration of the rewriting procedure of LIG on PI/PDMS composite substrate. **c** The dependence of the resistance of LIG formed on PI/PDMS composite substrate on the rewrite time (the error bars represent the standard deviations). The LIG are fabricated repeatedly onto the same PI/PDMS composite substrate under the condition of (specific power, frequency, scanning speed, DPI) = (12%, 16 kHz, 200 mm s^{-1}, 500). And the weight ratio of PI particles to PDMS is 1:2.

effectively increase the carbon content by over 4.68%. After pouring the mixture into the mold and curing at 55 °C for 2 h in sequence, the PI/PDMS composite films with a considerable carbon content are prepared. Then the laser scanning onto the surface of the composite films causes the carbonation of the PI particle, resulting in the remarkable electrical conductivity along the trace of laser induction patterned according to the digital model in the CAD file. After painting the conductive silver as the electrode to the two sides of regions of LIG and soldering metal wires on it, the fabrication of a soft and stretchable LIG-based piezoresistive sensor is completed. Supplementary Fig. 3b, presents the experimental image of this laser scanning procedure. The film in yellow is the PI/PDMS composite substrate, whose two ends are fixed to maintain its flatness when exposed to a sharp temperature increase. Moreover, Supplementary Fig. 3c gives the schematic illustration and the manufacturing parameters, where LIG is prepared in unidirectional scanning mode (from left to right). Here, the scanning speed equals to the moving speed of the laser head, and the red lines in the right subfigure represent the scanning tracks. The continuous and repeated scanning from left to right and the dense tracks along the vertical direction enables the LIG formation in this rectangle region. In general, the manufacturing parameters are divided into two categories, the material composition (i.e., the weight ratio of PI particle to PDMS) and the conditions of the laser scanning procedure (i.e., laser

power, frequency, scanning speed and DPI). All of them offer strong influences on the electrical and mechanical performances of this LIG-based system. The resistance variations as the increase of tensile strain or bending deflection for the specimens with different PI particle to PDMS weight ratios (i.e., 1:2, 1:3, and 1:4 from left to right) are measured, as illustrated in Fig. 2a. As the tensile strain increases, the resistance increases proportionally for specimen with a higher PI to PDMS weight ratio (i.e., 1:2), while increases nonlinearly for the ones with lower PI to PDMS weight ratios (i.e., 1:3 and 1:4) due to the gradual formation of crack in LIG. In addition, the gauge factor (GF), a critical parameter to evaluate the sensitivity of the piezoresistive sensors, is calculated using GF = ($\Delta R/R_0$)/ε, where ΔR, R_0, and ε denote the variation of the resistance, original resistance once fabricated and the applied strain, respectively. Thus 470% linear increase of the normalized resistance with a 15% tensile strain yields a constant gauge factor (i.e., 30) for the specimen with a 1:2 PI to PDMS weight ratio, which is an indispensable feature for its application in monitoring the external deformation. However, for the specimen with a lower PI to PDMS weight ratio, the gauge factor is in a relatively small value (i.e., 46 and 75 for specimens with 1:3 and 1:4 PI to PDMS weight ratio) at the beginning of tension, and increases sharply after a 6% tension before the broken of LIG at 10%. Though their remarkable sensitivity at a sizeable mechanical deformation, the narrow available strain window and the inconstant gauge factor set

constraints on their applications. Notably, a high PI concentration yields a wide available sensing range and a stable piezoresistive performance when exposed to an external mechanical deformation. Additionally, the durability of the LIG-based sensors on PI/PDMS substrate with different weight ratios (i.e., 1:2, 1:3, and 1:4 from left to right) are also experimentally studied, as shown in Fig. 2a. These specimens exhibit a good cyclability in the normalized resistance under different max strain values (i.e., 15%, 6%, and 4%). More results about the resistance and the corresponding SEM images of the LIG fabricated on PI/PDMS composite substrates can be found in Supplementary Fig. 4. The resistance of this soft and stretchable system decreases as the increase of the PI particle concentration but is almost a constant as the variation of PI particle size (as shown in Supplementary Fig. 4a), which can also be observed from SEM images illustrated in Supplementary Fig. 4b. And the PI particle size is chosen as 500 mesh (i.e., 25 μm). The larger of the PI content, the denser 3D porous graphene is formed under the irradiation of laser beam. For the linear resistance response of LIG based on PI/PDMS composite, the underlying mechanism lies in the Poisson's effect. The geometrical reduction of the cross-sectional area is induced by the tensile strain along the axial direction of the specimen. The compression between the 3D porous graphene in the cross-section due to the reduction of the cross-sectional area leads to the variation of the conductivity of the functional material with a higher PI/PDMS ratio (i.e., 1:2) and denser porous graphene. Thus, this obviously increased conductivity due to the Poisson's effect on the specimen with a higher PI/PDMS ratio (i.e., 1:2) mitigated the nonlinear increase in resistance due to the tensile strain-induced LIG crack.

Furthermore, the electronic performances and the durability of this flexible sensor are also studied through the outward and inward bending deformations (as shown in Supplementary Fig. 5). Notably, a stable response of the normalized resistance as the tensile and bending cycle increases (as shown in Supplementary Fig. 6) demonstrates the capability of this soft and stretchable LIG-based sensor in serving as a wearable electronical device. The mechanical performances of PI/PDMS composites with different weight ratios are given in Supplementary Fig. 7, and their elastic modulus. As the PI to PDMS weight ratio increases from 0:1 to 1:2, the modulus of the specimens increases nonlinearly. The bubbles generated during the mixing process could not be completely eliminated for the PI/PDMS solution with a high weight ratio (i.e., 1:1.5), yielding a specimen with lots of voids after 2 h of curing at 55 °C. Thus, the specimen with a higher PI/PDMS weight ratio (i.e., 1:1.5) exhibits a reduced modulus. Notably, the PI to PDMS weight ratio is chosen as 1:2 throughout this work unless specified, considering its linear response of normalized resistance to tensile strain. In particular, the LIG sensor fabricated on the PI/PDMS composite substrate is erasable and rewritable, promising its recycle attribute in practical applications. As shown by the schematic illustration in Fig. 2b, the LIG can be reformed on the same region of PI/PDMS composite substrate after removing the pre-prepared LIG with the common scotch tape, illustrating a good reproducibility. Figure 2c depicts the results of rewriting experiments at the same preparation parameters (i.e., specific power, frequency, scanning speed, DPI = 12%, 16 kHz, 200 mm s−1, 500) on three different specimens prepared from different batches but with the same PI/PDMS ratio 1:2. The error bars in Fig. 2c represent the standard deviations of testing results from different specimens. The maximum standard deviation (i.e., 24.5 Ω) relative to the mean value (i.e., 217 Ω) is 11.2%. Compared to LIG based on commercial PI films reported previously, which maximum standard deviation (i.e., 1.5 Ω) relative to the mean value (i.e., 18 Ω) is 8.3%[6]. Although the reproducibility of LIG based on PI/PDMS composite is slightly lower than that based on commercial PI, and it can be considered to have good reproducibility. The corresponding experimental optical photos are given in Supplementary Fig. 8. In particular, the stable resistance of LIG formed in different rewrite cycles but with

fixed manufacturing condition reveals the capability of this sensor in immediately recycling and reusing once damaged.

Study of manufacturing parameters on the conductivity of LIG

The manufacturing parameters during the laser scanning procedure are experimentally investigated. Figure 3 depicts the effects of the laser power and frequency on the resistance of LIG. The dimensional size of the LIG region demonstrated here is 10 mm × 10 mm, and the weight ratio of the PI particle to PDMS is fixed as 1:2. The specific power value and the frequency of the laser are determined by the waveform of pulse width modulation (PWM) controller. The laser always outputs at maximum power (i.e., 30 W). The duty ratio of the waveform is equal to the percentage of the maximum laser output power (i.e., the actual working time of the laser), and the frequency of the waveform is similar to the laser frequency (i.e., the number of laser pulses in one second). Figure 3a gives the contour plot of the resistance in terms of specific power and frequency. As illustrated in Fig. 3b, the resistance of LIG decreases as the laser power increases before reaching its minimum value at 12%, beyond which the resistance increases then. In contrast, the resistance of LIG shows a monotonical dependence on the frequency and decreases from 1600 Ω to 180 Ω as the frequency increases from 8 kHz to 20 kHz (as shown in Fig. 3c). All these phenomena can also be observed and explained from the micro level by the SEM images shown in Fig. 3d. The top four images are the micrographs of the LIG formed under the same frequency (i.e., 16 kHz) but different specific power values (i.e., 8%, 12%, 16%, and 20% from left to right). In comparison, the bottom left three images are the ones formed under a fixed specific power (i.e., 12%) but different frequency values (i.e., 8 kHz, 12 kHz, and 20 kHz from left to right). In general, a high laser power brings more energy inputs per unit area, leading to the damage of the PI/PDMS composite substrate and without continuous LIG formation (e.g., the case of 20%-16 kHz). In contrast, a low laser power yields an insufficient energy input to convert the carbon source in PI to porous graphene, where the sample remains mainly in the form of carbonization lamella (e.g., the case of 8%-16 kHz). Here, 12% and 16% represent the two optimized specific power values for the fixed frequency of 16 kHz, which also can be derived from the dense and uniform distribution of the porous graphene in the corresponding SEM images. The frequency higher than the threshold value (i.e., 12 kHz for a fixed specific power of 12%) is required to form the conductive LIG. However, the further increase of the frequency does not seem to affect its conductivity. The apparent defects on the surface of porous graphene observed in the SEM images for specimens formed under a lower frequency (i.e., 8 kHz) lead to the higher resistance of LIG, while the higher frequencies (i.e., 12 kHz to 20 kHz) yield the decreasing resistance. Visible porous graphene structures can be seen in the enlarged image at the lower right corner of Fig. 3d. During laser induction, PI particles are irradiated by a pulsed laser. As a result of rapid outgassing, the PI particles expand, and their surfaces break up to release gas, forming spherical particles made of 3D fibers. This process is similar to the preparation of LIG on the surface of the PI film[16,52]. By comparing LIG prepared at different specific power values (i.e., 8% to 20%), it can be found that more considerable instantaneous expansion of PI particles and 3D porous graphene particles forms by the greater laser thermal radiation as the increase of laser specific power. More details about the influences of the specific power and frequency on the resistance or conductivity of the LIG can be found from the SEM images with different magnifications in Supplementary Fig. 9. Notably, the specific power and frequency during the laser scanning procedure are finally determined as 12% and 16 kHz, respectively.

Furthermore, the electrical performance of LIG not only depends on the output of laser generator, but is also highly
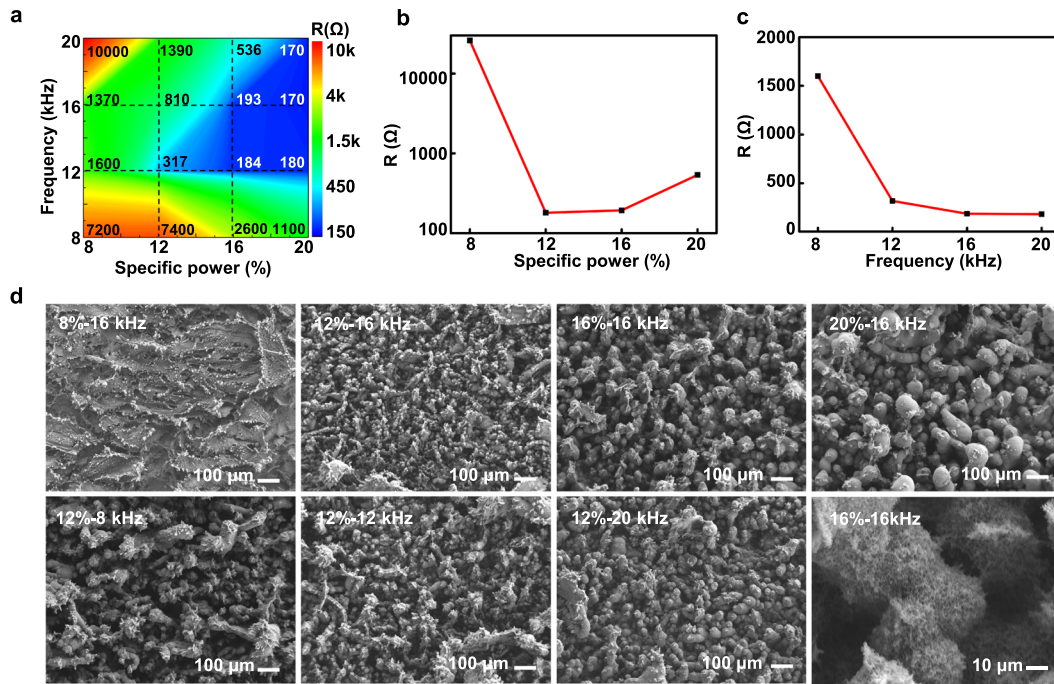
Fig. 3 Dependences of the resistance of LIG fabricated on the PI/PDMS composite substrate on the specific power and frequency. a Contour plot of the resistance in terms of specific power value and frequency. **b** The variation of the resistance with the increase of specific power but a fixed frequency (16 kHz). **c** The variation of the resistance with the increased frequency but a fixed specific power (12%). **d** SEM images of LIG fabricated under different specific power values and frequencies. The scanning speed and DPI are fixed as 200 mm s^{-1} and 500. And the weight ratio of PI particles to PDMS is 1:2.

related to the distribution of laser pulses. The scanning speed and dots per inch (DPI) represent two critical parameters during the laser scanning procedure, whose effects on the conductivity of LIG are illustrated in Fig. 4. Here, the parameter of dots per inch (DPI) represents the density of laser scanning tracks along the vertical direction. For a given laser power (P), the relationship between the dots per inch (DPI), and scanning speed (V), and the fluence of the laser (H), can be expressed as

$$H = \frac{P \cdot \text{DPI}}{V} \qquad (1)$$

From Eq. (1), the high laser power, the large DPI coupled with the low scanning speed yields a more energy inputs per unit area. Notably, the fluence of the laser during the scanning procedure is experimentally determined as the only critical parameter to control the formation of porous graphene on the PI/PDMS composite substrate. It is a handy tool in the selection of the optimized collection of manufacturing parameters. Figure 4b gives a contour plot of the resistance of LIG in terms of scanning speed and DPI and shows that a smaller scanning speed coupled with an optimized DPI results in a higher conductivity for a given laser specific power (i.e., 12%) and frequency (16 kHz). Despite the various manufacturing parameters during the directly writing procedure, the fluence of the laser herein is determined as the only principle to characterize the formation of LIG on PI/PDMS composites substrate. More specifically, the dash lines in this contour plot represent the manufacturing conditions of LIG on PI/PDMS composite substrate with the same H under different scanning speeds and DPI values. Here, the maximum and minimum fluence of the laser to achieve a conductive LIG (i.e., R < 2000 Ω) are 141.6 J cm^{-2} and 26.5 J cm^{-2}, respectively. For the case of a low DPI (e.g., 500) coupled with a high scanning speed (e.g., 400 mm s^{-1}), the fluence of the laser is about 17.7 J cm^{-2}, smaller than the minimum fluence to convert the carbon in PI/PDMS composite substrate to porous graphene. As observed in the corresponding SEM image shown in the upper right corner of

Fig. 4c, only some lamellar ablative product is formed under the irradiation of laser beam, without any formation of typical porous graphene. The PI film is known for its oxygen and nitrogen outgassing at 550 °C, then carbonization at 700 °C, and finally graphitization at 3000 °C[55,56]. Therefore, when the fluence of the laser is insufficient, the surface of the composite is subjected to the low irradiation and cannot be instantly heated up to the transition temperature of PI to graphene. As the scanning speed decreases from 400 mm s^{-1} to 100 mm s^{-1} with a fixed DPI of 500, it can be found from the corresponding SEM images shown in Fig. 4c, Supplementary Fig. 10c and Supplementary Fig. 11, that the porosity of the PI/PDMS composite substrate increases, thereby increasing the conductivity of the fabricated LIG-based sensor. Under another fixed preparation parameter condition (the specific power value, frequency, and DPI are fixed as 18%, 16 kHz, and 1000). Similar change in resistance values and SEM images as the scanning speed increases from 100 mm s^{-1} to 500 mm s^{-1} are shown in Supplementary Fig. 12, demonstrating the rationality of the above analysis. In contrast, the excessive power input that beyond the maximum value of the fluence of the laser leads to the gradual ablation and emerging damages of the soft and stretchable composite substrate. For the case of a high DPI (e.g., 1500) coupled with a low scanning speed (e.g., 100 mm s^{-1}), a high fluence of the laser (i.e., 212.6 J cm^{-2}), which substantially exceeds the maximum value of 141.6 J cm^{-2}, yields the apparent cracks and the discontinuous of the fabricated porous graphene on the surface of the PI/PDMS composite substrate. In this condition, the LIG has slight electrical conductivity and is labeled as 10000 Ω for comparison with other samples. As summarized in Fig. 4c and Supplementary Fig. 10a, the disappearing cracks and increasing porosity of the PI/PDMS composite substrate decrease the resistance of the fabricated LIG, as the scanning speed increases from 100 mm s^{-1} to 500 mm s^{-1} for a fixed DPI of 1500. Similarly, the excessive value of DPI will lead to overmuch laser energy output and affect the conductivity of LIG. As summarized in Fig. 4c and Supplementary Fig. 10b, SEM images show the
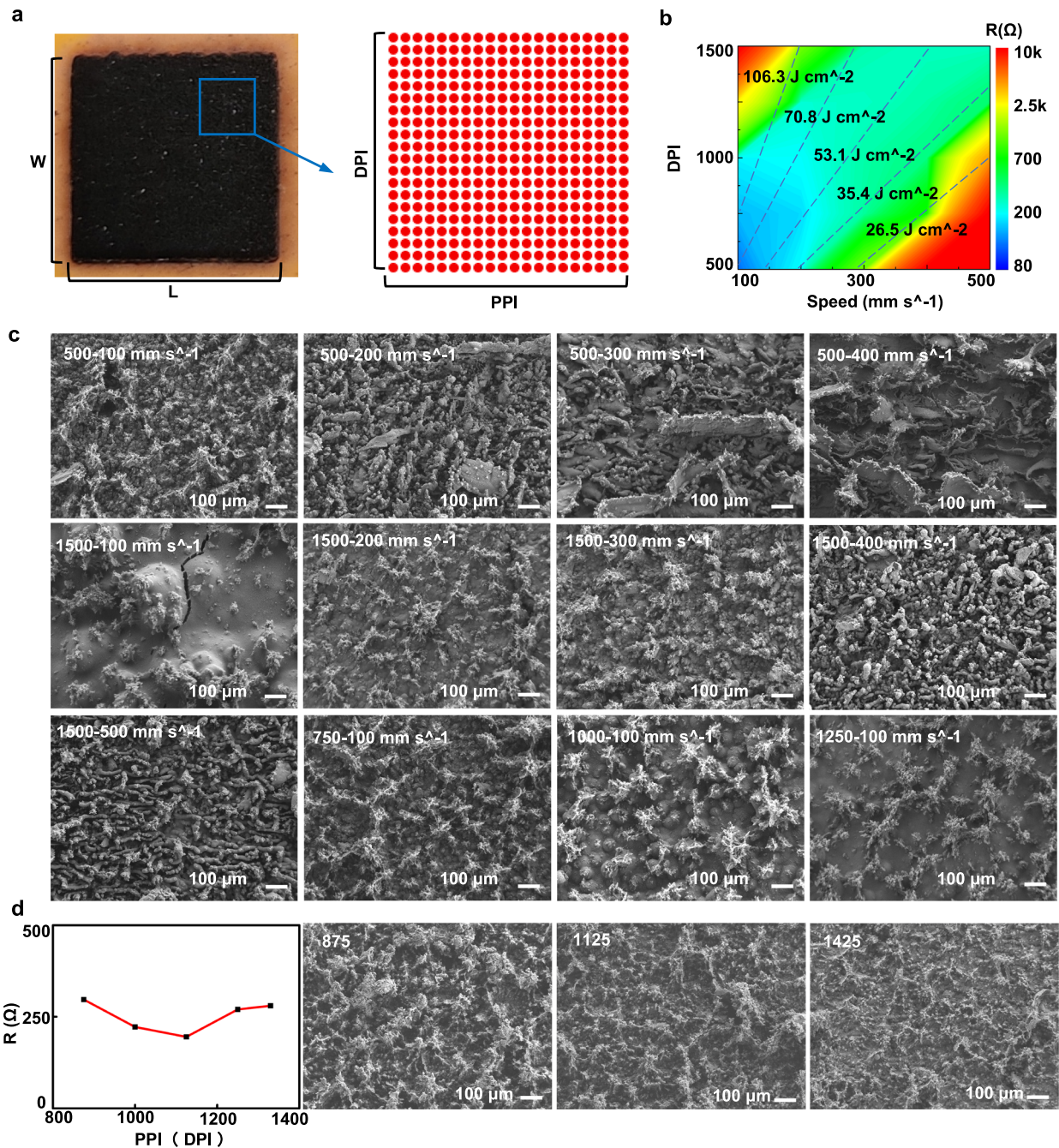
Fig. 4 Dependences of the resistance of LIG on scanning speed and dots per inch (DPI). a Schematic illustration of the DPI and PPI during the laser scanning procedure. **b** The contour plot of the resistance of LIG in terms of scanning speed and DPI. **c** SEM images of LIG fabricated under different speeds and DPI values. The specific power and frequency are fixed as 12% and 16 kHz. And the weight ratio of PI particles to PDMS is 1:2. **d** Dependences of the resistance of LIG on PPI and DPI. SEM images of LIG fabricated under a fixed fluence of the laser (70.8 J cm^{-2}) but different frequencies, scanning speeds and DPI values. The LIG is fabricated onto PI/PDMS composite substrate under the condition of (specific power, frequency, scanning speed, DPI) = (12%, 6 kHz, 175 mm s^{-1}, 875), (12%, 10 kHz, 225 mm s^{-1}, 1125), and (12%, 16 kHz, 285 mm s^{-1}, 1425), from left to right. And the weight ratio of PI particles to PDMS is 1:2.

decreasing density of 3D porous graphene on the PI/PDMS composite substrate as the DPI increases from 500 to 1500 for a fixed scanning speed of 100 mm s^{-1}. Even the surface is damaged by severe thermal deformation at DPI of 1500. This phenomenon leads to the decrease of the conductivity of LIG or even close to the broken circuit. More details about the influences of the scanning speed and DPI on the resistance or conductivity of the fabricated LIG in the aspect of the fluence of the laser can be found from the SEM images with different magnifications in

Supplementary Fig. 10c and Supplementary Fig. 11. Though a wide range of the laser fluence bringing a conductive LIG (i.e., from 26.5 J cm^{-2} to 141.6 J cm^{-2}), the resistances of the specimens formed under the specific condition in this range are still high (e.g., the fluence of the laser, resistance = 26.5 J cm^{-2}, 800 Ω or 106.3 J cm^{-2}, 1290 Ω). Thus, it is necessary to give a relatively smaller laser fluence range according to the resistance contour plot in Fig. 4b. Finally, the reasonable range of laser fluence is from 35.4 J cm^{-2} to 70.8 J cm^{-2}, and is determined from the blue and

light green areas of contour plot in which the resistances of LIG are less than 500 Ω.

In general, the laser scanning procedure essentially forms of continuous pulse dots on a substrate following a preset trajectory. As shown in Fig. 4a, the red dots represent the matrix of laser pulses, and the distribution densities along the horizontal and vertical direction are given by the pulses per inch (PPI) and the dots per inch (DPI), respectively. By definition, the pulses per inch (PPI) can be expressed given by F/V. Here, F and V represent the frequency of laser pulse and scanning speed, respectively. Thus the fluence of the laser (H) can be expressed as

$$H = \frac{P \cdot DPI \cdot PPI}{F} \qquad (2)$$

As shown in Fig. 4d, the LIG were formed under the same H value (i.e., 70.8 J cm^{-2}) but different PPI and DPI values (i.e., 875, 1000, 1125, 1235, and 1425). In order to change the PPI value and DPI value simultaneously and keep a fixed H value, the scanning speed, laser frequency, and DPI are required to be adjusted at the same time. Thus, we summarize the resistance of LIG obtained under the same fluence of the laser but different pulse distributions. From their corresponding resistances shown in the left subfigure of Fig. 4d, the resistances of LIG are in a stable range and have good conductivity. The representative SEM images of LIG are located on the right side of Fig. 4d, fabricated under different PPI values (i.e., 875, 1125, 1425 from left to right) but a fixed H value of 70.8 J cm^{-2}. At the same fluence of the laser, the dense laser distribution means a higher PPI (DPI) value, but the energy contained in each pulse is lower, which is reflected in a denser distribution of porous graphene and smaller size of porous graphene in microscopic morphology. Both the larger size and the higher density of porous graphene can effectively reduce resistance. As shown in the SEM images of Fig. 4d, the decreasing size of porous graphene but increasing density of porosity of fabricated LIG on PI/PDMS composite substrate exhibit an approximate conductivity, as the PPI and DPI values increase from 875 to 1425 for a fixed H value of 70.8 J cm^{-2}. From Eqs. 1 and 2, the fluence of the laser is theoretically determined as the only principle in selecting the optimized collection of the manufacturing parameters, greatly facilitating the fabrication procedure of the conductive LIG on the soft and stretchable PI/PDMS composite substrate. To achieve a soft and stretchable LIG-based sensor with a remarkable conductivity, the optimized manufacturing parameters including the specific power, the frequency, the scanning speed and DPI are determined as 12%, 16 kHz, 200 mm s^{-1} and 500, respectively.

Applications of LIG-based sensors

Considering its combined attributes of the stable electrical performance, the remarkable stretchability, the high sensitivity and the linearity of resistance to the external mechanical deformation, the LIG-based sensors stand out as the prominent candidate of functional material for wearable electronics to monitor human motions and physical activities continuously, or for the wearable remote controller of actuators. Here, the variation in the normalized resistance due to the piezoresistive effect is utilized to predict the human electrophysiological activities. From Fig. 5a, a stable and high-quality pulse rate signal such as percussion wave (P), tidal wave (T), and diastolic wave (D) is recorded immediately after the soft sensor adhered onto the wrist of a volunteer[18,57,58]. The pulse wave is a critical physiological signal that reflects the body's condition, and 71 beats per minute reveals a healthy condition of this volunteer. Furthermore, a variety of soft and stretchable LIG-based sensors fabricated on PI/PDMS composites substrate can be designed to monitor the human motion and remote controllers of robots. As illustrated in Fig. 5b, the motions of the left index finger can be timely

monitored and preciously predicted through the LIG sensors adhered onto the three joints, including the metacarpophalangeal point (MP), proximal interphalangeal point (PIP) and distal interphalangeal point (DIP) from the palm to the fingertip. Figure 5c depicts the experiment of the demonstration of the fabricated LIG-based sensor on PI/PDMS composite substrate as the remote real-time wearable controller of a LIG actuator. The complete experiment process is shown in Supplementary Movie 1. More specifically, a wearable soft glove is fabricated utilizing the mixture solution of PDMS and PI particles by the demolding approach, as illustrated in Supplementary Fig. 13. This soft glove with separate LIG sensors holds the promise for monitoring the finger motion and even the gestures by analyzing the coupled motions of the five fingers. As summarized in Fig. 5d and Fig. 5e, a set of typical gestures can be recognized by measuring the real-time resistances of the LIG sensors on the wearable glove, including the ones for 0 to 5 and the ones of the Rock-Paper-Scissors game. Furthermore, this functional glove can also serve as a wearable controller for the remote control of actuators, demonstrating its potential in soft robots (as shown in Fig. 5f and Supplementary Movie 2).

DISCUSSION

In conclusion, we had successfully prepared LIG on the PI/PDMS composite substrate under the irradiation of an infrared laser beam. Ascribing to the flexible and stretchable properties of the PI/PDMS substrate, the LIG-based sensors show the capability to match complex 3D shapes and bear a mechanical tension over 15%, which is greater than the elasticity of human skin, while maintaining the stability in their electrical performances. Notably, an 470% linear increase and good cyclability of the normalized resistance for a 15% tensile strain shows an indispensable feature for its application in human motion monitoring. Manufacturing parameters, including composite preparation parameters (PI particle concentration and PI particle size) and laser scanning parameters (i.e., laser power, frequency, scanning speed, and DPI), are systematically studied to reveal their influences on the electrical properties of soft and stretchable LIG-based sensing systems. Notably, the fluence of the laser is experimentally and theoretically determined as the only principle to characterize the formation of conductive LIG on PI/PDMS composite substrate, greatly facilitating the selection of the laser scanning parameters with the given optimized fluence. Moreover, the reasonable range of the laser fluence to achieve the LIG-based sensor with an available electronical performance is finally determined as from 35.4 J cm^{-2} to 70.8 J cm^{-2}. Furthermore, three demonstration examples, including the sensor of electrophysiological activities sensing, the monitor of finger motion, and the tool of remote gesture control, are conducted to highlight the remarkable sensitivity, the good cyclability and the inherent stretchability of the LIG-based electrical system. These characteristics demonstrated in this manuscript promise the soft and stretchable LIG-based system's capability to serve as the critically functional component of flexible and wearable electronics.

METHODS

PI/PDMS composite preparation

The PI/PDMS composite preparation began with the mixing PDMS (Sylgard 184, Dow Corning) with prepolymer and hardener in a 10:1 mass ratio. Then, PI particles (500, 800, and 1000 mesh, Dupont) were added into mixed PDMS solution with a specific mass ratio (i.e., 1:4, 1:3, and 1:2). After a 30 min stirring by an electric mixer and 1 h laying in a vacuum drying oven at room temperature to remove bubbles, the mixture consisting of PDMS and PI particles was poured into the pre-designed mold and is cured at 55 °C for 2 h in sequence. Then, the PI/PDMS composite films with sufficient carbon source were fabricated.
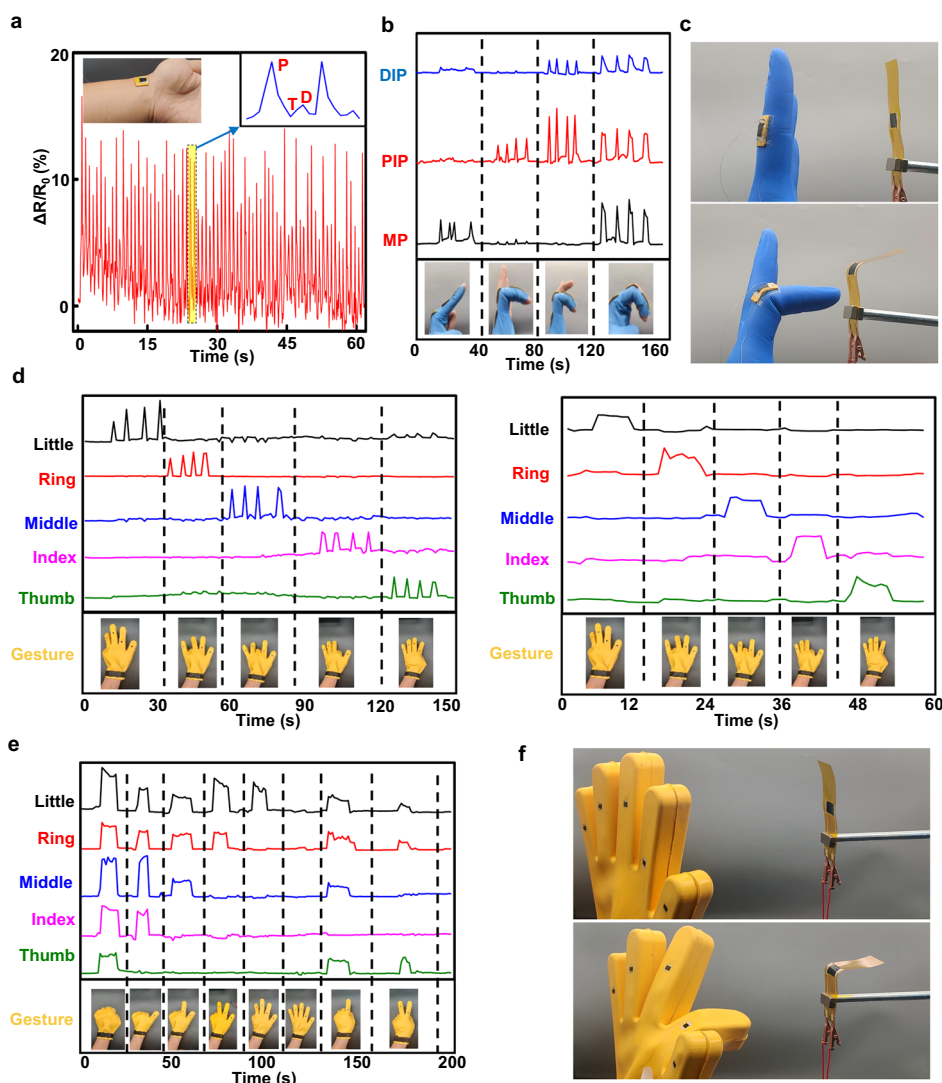
Fig. 5 The application of the soft and stretchable LIG-based sensors. a The pulse rate wave recorded by the soft and stretchable LIG-based sensor adhered onto the wrist. **b** The real-time feedback for the joint motions of one index finger. **c** Demonstrations of the LIG-based sensor as a tool to remotely control the bending motion of an actuator. **d** Real-time feedback for motions of the five fingers of the left hand in sequence with the LIG-based wearable glove. **e** Recognition of typical gestures with the LIG-based wearable glove. **f** Demonstrations of the LIG-based wearable glove for the remote control of a soft robot. The LIG-based sensor is fabricated onto PI/PDMS composite substrate under the condition of (specific power, frequency, scanning speed, DPI) = (12%, 16 kHz, 200 mm s^{-1}, 500). And the weight ratio of PI particle to PDMS is 1:2.

Fabrication of porous LIG on PI/PDMS composite substrate

The prepared PI/PDMS substrate was placed on the commercial laser cutting platform (X-7050, G.U. Eagle Automation), whose two ends were fixed to maintain its flatness when exposed to a sharp temperature increase. The maximum power of the laser cutting machine equipped with a CO$_2$ laser generator is 30 W. LIG were made with a fixed focal length (i.e., 10 mm), same scan mode (i.e., one-way scan mode, from left to right) and same dimensional size (i.e., rectangular area: 10 mm × 10 mm).

Fabrication of the soft and stretchable LIG-based sensor

LIG was prepared on a rectangle PI/PDMS composite substrate under the specific power of 12%, the laser frequency of 16 kHz, the scanning speed of 200 mm s^{-1}, the DPI of 500. The dimensional size of the LIG region was 20 mm × 10 mm and the weight ratio of PI particle to PDMS of specimens was 1:2. After painting the conductive silver to the two sides of regions of LIG as the electrodes, the fabrication of a soft and stretchable LIG-based piezoresistive sensor was completed.

Fabrication of the soft and stretchable PI/PDMS composite glove

The fabrication of the soft and stretchable PI/PDMS composite glove began with pouring the composite mixture solution into the PTFE glove mold, and the weight ratio of PI particle to PDMS of mixture solution was 1:2. After fully curing in the drying oven at 55 °C for 2 h, one half of the soft and stretchable PI/PDMS composite glove was fabricated. A soft and stretchable PI/PDMS composite glove was successfully prepared after combing the two half parts of glove. LIG-based sensors were prepared on PI/PDMS composite glove under the specific power of 12%, the laser frequency of 16 kHz, the scanning speed of 200 mm s^{-1}, the DPI of 500. The dimensional size of the LIG region was 5 mm × 5 mm.

Fabrication of the actuator composed of PI film and PDMS

The fabrication process of actuators began with the direct laser scanning of LIG on a thin PI film. After the preparation of LIG, conductive silver was painted onto the two sides of LIG region as electrodes, and then the PDMS solution was spin-coated on the sample surface with a spin coating speed

of 400 RPM and a spin coating time of 100 seconds. After the PDMS curing, the fabrication of the actuator was completed.

Measurement of the soft and stretchable LIG-based sensor

The SEM images were taken by Zeiss Sigma 300, and the variation of the resistance was recorded by the digit multimeters (i.e., 34465 A, KEYSIGHT; HPS5124, Helpass). Tensile and bending experiments were conducted on a universal mechanical testing machine, and the specific dimensional size of the PI/PDMS composite specimen is 75 mm × 20 mm × 1.5 mm. Pulse and throat motion monitor experiments were conducted by the digit multimeters with a sampling rate of 2 Hz (i.e., 34465 A, KEYSIGHT). The LIG-based sensor was attached to the volunteers' wrist and throat by common double-sided tape, and the specific dimensional size of the PI/PDMS composite specimens were 20 mm × 20 mm × 0.5 mm and 60 mm × 40 mm × 0.5 mm, respectively. Finger motion and gesture monitor experiments were conducted by the digit multimeters with a sampling rate of 1 Hz (i.e., HPS5124, Helpass). The specific dimensional size of PI/PDMS composite specimens attached to the index finger of a commercial latex glove was 20 mm × 15 mm × 1 mm. In the remote-control experiments, the input and output terminals of SCM were connected with the DC power supply (i.e., IT6720, ITECH) and the actuator, respectively. And the control terminal of SCM was connected with the sensors (i.e., LIG-based sensors on joints and wearable PI/PDMS composite glove).

In experiments with volunteers, we have complied with all relevant ethical regulations. The experiments involving human subjects have been performed with the full, informed consent of the volunteers.

DATA AVAILABILITY

The experimental data referenced in this text is available from the corresponding authors upon reasonable request.

REFERENCES

1. Ye, R. et al. Laser-induced graphene formation on wood. *Adv. Mater.* **29**, 1702211 (2017).
2. Le, T. S. D., Park, S., An, J., Lee, P. S. & Kim, Y. J. Ultrafast laser pulses enable one-step graphene patterning on woods and leaves for green electronics. *Adv. Funct. Mater.* **29**, 1902771 (2019).
3. Wang, H. et al. Laser writing of Janus graphene/kevlar textile for intelligent protective clothing. *ACS Nano* **14**, 3219–3226 (2020).
4. Li, Z. et al. Preparation of laser-induced graphene fabric from silk and its application examples for flexible sensor. *Adv. Eng. Mater.* **23**, 2100195 (2021).
5. Chyan, Y. et al. Laser-induced graphene by multiple lasing: toward electronics on cloth, paper, and food. *ACS Nano* **12**, 2176–2183 (2018).
6. Lin, J. et al. Laser-induced porous graphene films from commercial polymers. *Nat. Commun.* **5**, 5714 (2014).
7. Yang, Y. et al. A laser-engraved wearable sensor for sensitive detection of uric acid and tyrosine in sweat. *Nat. Biotechnol.* **38**, 217–224 (2020).
8. Chen, J., Wang, Y., Liu, F. & Luo, S. Laser-induced graphene paper heaters with multimodally patternable electrothermal performance for low-energy manufacturing of composites. *ACS Appl. Mater. Interfaces* **12**, 23284–23297 (2020).
9. Kaidarova, A. et al. Laser-printed, flexible graphene pressure sensors. *Glob. Chall.* **4**, 2000001 (2020).
10. Kaidarova, A. et al. Wearable multifunctional printed graphene sensors. *npj Flex. Electron.* **3**, 15 (2019).
11. Song, W. et al. Flexible, stretchable, and transparent planar microsupercapacitors based on 3D porous laser-induced graphene. *Small* **14**, 1702249 (2018).
12. Wang, Y., Wang, Y., Zhang, P., Liu, F. & Luo, S. Laser-induced freestanding graphene papers: a new route of scalable fabrication with tunable morphologies and properties for multifunctional devices and structures. *Small* **14**, 1802350 (2018).
13. Li, L. et al. High-performance pseudocapacitive microsupercapacitors from laser-induced graphene. *Adv. Mater.* **28**, 838–845 (2016).
14. Nayak, P., Kurra, N., Xia, C. & Alshareef, H. N. Highly efficient laser scribed graphene electrodes for on-chip electrochemical sensing applications. *Adv. Electron. Mater.* **2**, 1600185 (2016).
15. Li, Y. et al. Laser-induced graphene in controlled atmospheres: from superhydrophilic to superhydrophobic surfaces. *Adv. Mater.* **29**, 1700496 (2017).
16. Duy, L. X. et al. Laser-induced graphene fibers. *Carbon* **126**, 472–479 (2018).
17. Ye, R., James, D. K. & Tour, J. M. Laser-induced graphene: from discovery to translation. *Adv. Mater.* **31**, 1803621 (2018).
18. Chen, X. et al. A dual-functional graphene-based self-alarm health-monitoring e-skin. *Adv. Funct. Mater.* **29**, 1904706 (2019).
19. Chen, Y. et al. UV laser-induced polyimide-to-graphene conversion: modeling, fabrication, and application. *Small Methods* **3**, 1900208 (2019).
20. Shi, X. et al. One-step scalable fabrication of graphene-integrated micro-super-capacitors with remarkable flexibility and exceptional performance uniformity. *Adv. Funct. Mater.* **29**, 1902860 (2019).
21. Zhang, Y. et al. Laser-induced graphene-based non-enzymatic sensor for detection of hydrogen peroxide. *Electroanalysis* **31**, 1334–1341 (2019).
22. Dallinger, A., Keller, K., Fitzek, H. & Greco, F. Stretchable and skin-conformable conductors based on polyurethane/laser-induced graphene. *ACS Appl. Mater. Interfaces* **12**, 19855–19865 (2020).
23. Gandla, S. et al. Highly linear and stable flexible temperature sensors based on laser-induced carbonization of polyimide substrates for personal mobile monitoring. *Adv. Mater. Technol.* **5**, 2000014 (2020).
24. Li, J. T., Stanford, M. G., Chen, W., Presutti, S. E. & Tour, J. M. Laminated laser-induced graphene composites. *ACS Nano* **14**, 7911–7919 (2020).
25. Ling, Y. et al. Laser-induced graphene for electrothermally controlled, mechanically guided, 3D assembly and human-soft actuators interaction. *Adv. Mater.* **32**, 1908475 (2020).
26. Wang, W. et al. Laser-induced graphene tapes as origami and stick-on labels for photothermal manipulation via marangoni effect. *Adv. Funct. Mater.* **31**, 2006179 (2020).
27. Duan, S. et al. Waterproof mechanically robust multifunctional conformal sensors for underwater interactive human-machine interfaces. *Adv. Intell. Syst.* **3**, 2100056 (2021).
28. Tham, N. C. Y. et al. Thermally controlled localized porous graphene for integrated graphene-paper electronics. *Adv. Mater. Technol.* **6**, 2001156 (2021).
29. Xu, K. et al. A wearable body condition sensor system with wireless feedback alarm functions. *Adv. Mater.* **33**, 2008701 (2021).
30. Yan, Z. et al. Flexible high-resolution triboelectric sensor array based on patterned laser-induced graphene for self-powered real-time tactile sensing. *Adv. Funct. Mater.* **31**, 2100709 (2021).
31. Ma, Y. et al. Flexible hybrid electronics for digital healthcare. *Adv. Mater.* **32**, 1902062 (2019).
32. Zang, X. et al. Laser-induced molybdenum carbide-graphene composites for 3D foldable paper electronics. *Adv. Mater.* **30**, 1800062 (2018).
33. Park, H., Kim, M., Kim, B. G. & Kim, Y. H. Electronic functionality encoded laser-induced graphene for paper electronics. *ACS Appl. Nano Mater.* **3**, 6899–6904 (2020).
34. Kulyk, B. et al. Laser-induced graphene from paper for mechanical sensing. *ACS Appl. Mater. Interfaces* **13**, 10210–10221 (2021).
35. Vashisth, A. et al. ReaxFF simulations of laser-induced graphene (LIG) formation for multifunctional polymer nanocomposites. *ACS Appl. Nano Mater.* **3**, 9b02524 (2020).
36. Sun, B. et al. Gas-permeable, multifunctional on-skin electronics based on laser-induced porous graphene and sugar-templated elastomer sponges. *Adv. Mater.* **30**, 1804327 (2018).
37. Zhu, J. et al. Laser-induced graphene non-enzymatic glucose sensors for on-body measurements. *Biosens. Bioelectron.* **193**, 113606 (2021).
38. Rahimi, R., Ochoa, M., Yu, W. & Ziaie, B. Highly stretchable and sensitive unidirectional strain sensor via laser carbonization. *ACS Appl. Mater. Interfaces* **7**, 4463–4470 (2015).
39. Xu, K. et al. Highly stable kirigami-structured stretchable strain sensors for per-durable wearable electronics. *J. Mater. Chem. C.* **7**, 9609–9617 (2019).
40. Zhang, C. et al. High-energy all-in-one stretchable micro-supercapacitor arrays based on 3D laser-induced graphene foams decorated with mesoporous ZnP nanosheets for self-powered stretchable systems. *Nano Energy* **81**, 105609 (2021).
41. Chen, Y. et al. Interfacial laser-induced graphene enabling high-performance liquid-solid triboelectric nanogenerator. *Adv. Mater.* **33**, 2104290 (2021).
42. Lu, B., Jin, X., Han, Q. & Qu, L. Planar graphene-based microsupercapacitors. *Small* **17**, 2006827 (2021).
43. Zhang, J. et al. Oxidized laser-induced graphene for efficient oxygen electrocatalysis. *Adv. Mater.* **30**, 1707319 (2018).
44. Alhajji, E., Zhang, F. & Alshareef, H. N. Status and prospects of laser-induced graphene for battery applications. *Energy Technol.* **9**, 2100454 (2021).
45. Ren, M., Zhang, J., Fan, M., Ajayan, P. M. & Tour, J. M. Li-breathing air batteries catalyzed by mnnife/laser-induced graphene catalysts. *Adv. Mater. Interfaces* **6**, 1901035 (2019).
46. Huang, L. et al. Highly efficient and rapid inactivation of coronavirus on non-metal hydrophobic laser-induced graphene in mild conditions. *Adv. Funct. Mater.* **31**, 2101195 (2021).

47. Zhu, F., Xiao, H., Li, H., Huang, Y. & Ma, Y. Irregular hexagonal cellular substrate for stretchable electronics. *J. Appl. Mech.* **86**, 034501 (2019).
48. Rogers, J. A., Someya, T. & Huang, Y. Materials and mechanics for stretchable electronics. *Science* **327**, 1603–1607 (2010).
49. Zhang, Y. et al. Printing, folding and assembly methods for forming 3D mesostructures in advanced materials. *Nat. Rev. Mater.* **2**, 17019 (2017).
50. Yan, D. et al. Soft three-dimensional network materials with rational bio-mimetic designs. *Nat. Commun.* **11**, 1180 (2020).
51. Yang, Z. et al. Conductive and elastic 3D helical fibers for use in washable and wearable electronics. *Adv. Mater.* **32**, 1907495 (2020).
52. Song, Z. et al. Kirigami-based stretchable lithium-ion batteries. *Sci. Rep.* **5**, 10988 (2015).
53. Parmeggiani, M. et al. PDMS/polyimide composite as an elastomeric substrate for multifunctional laser-induced graphene electrodes. *ACS Appl. Mater. Interfaces* **11**, 33221–33230 (2019).
54. Lamberti, A., Clerici, F., Fontana, M. & Scaltrito, L. A highly stretchable supercapacitor using laser-induced graphene electrodes onto elastomeric substrate. *Adv. Energy Mater.* **6**, 1600050 (2016).
55. Inagaki, M., Meng, L.-J., Ibuki, T., Sakai, M. & Hishiyama, Y. Carbonization and graphitization of polyimide film "Novax". *Carbon* **29**, 1239–1243 (1991).
56. Inagaki, M. et al. Carbonization of polyimide film "Kapton". *Carbon* **27**, 253–257 (1989).
57. Ma, Y. et al. Relation between blood pressure and pulse wave velocity for human arteries. *Proc. Natl Acad. Sci. USA* **115**, 11144–11149 (2018).
58. Jin, Y. et al. Identifying human body states by using a flexible integrated sensor. *npj Flex. Electron.* **4**, 28 (2020).

ACKNOWLEDGEMENTS

AUTHOR CONTRIBUTIONS

All authors contributed to the preparation of this paper. X.G. and H.W. conceived the research idea. They co-wrote the manuscript with contributions from all authors. X.G. supervised the overall project. H.W., Z.Z., and P.L. conducted the composite preparation and electrical characterization experiments. H.W. and Z.Z. drawn the schematic illustrations and carried out the SEM observance. H.W. and P.L. fabricated the sensors and studied their applications. Z.Z. and P.L. helped in the realization of electronics and the analysis of experimental data.

COMPETING INTERESTS

The authors declare no competing interests.

ADDITIONAL INFORMATION

Supplementary information The online version contains supplementary material available at https://doi.org/10.1038/s41528-022-00161-z.

Correspondence and requests for materials should be addressed to Xiaogang Guo.

Reprints and permission information is available at http://www.nature.com/reprints

Publisher's note Springer Nature remains neutral with regard to jurisdictional claims in published maps and institutional affiliations.